SUPPORTING MATERIAL

Solid state interactions in the La-Au-Mg system: phase equilibria, novel compounds and chemical bonding

R. Freccero[1,2], S. De Negri[1,*], A. Saccone[1], P. Solokha[1]

[1]Dipartimento di Chimica e Chimica Industriale, Università degli Studi di Genova, via Dodecaneso 31, 16146 Genova, Italy

[2]Max-Planck-Institut für Chemische Physik fester Stoffe Nöthnitzer Straße 40, 01187 Dresden (Germany) (present address)

Literature data on the La-Au-Mg system in the range of interest

The La-Mg, La-Au (≥ 50 at.% La) and Mg-Au (≥ 75 at.% La) binary boundary systems are briefly commented in the following. The recently reviewed[1] La-Mg binary system, includes six intermetallic phases (LaMg, $LaMg_2$, $LaMg_3$, La_2Mg_{17}, La_5Mg_{41}, and $LaMg_{12}$), all forming peritectically except for $LaMg_3$ (*cF*16-BiF_3) which forms congruently. Two of these phases, $LaMg_2$ (*cF*24-$MgCu_2$) and La_5Mg_{41} (*tI*92-Ce_5Mg_{41}) are reported to decompose at 725 and about 600 °C respectively, in agreement with previous data.[2,3] The crystal structures of the La-Mg binary phases are generally well assessed, nevertheless, two of them were recently re-determined: the La_2Mg_{17} phase, previously reported as *hP*38-Th_2Ni_{17}, was assigned to the disordered $CeMg_{10.3}$ prototype,[4] and the $LaMg_{12}$ phase, usually ascribed to the tetragonal $ThMn_{12}$ structure type, was instead found to be orthorhombic with a giant unit cell, and stoichiometry of $LaMg_{\sim 11}$.[5]

The La-Au intermetallic compounds involved in our investigation are La_2Au and LaAu.[6,7] They form peritectically at 668°C ($LaAu_2$) and by congruent melting at 1323°C (LaAu). The LaAu presents two crystalline forms, the HT form, *oS*8-TlI type, at temperature higher than 660 °C and the LT form, *oP*8-FeB. The possible existence of the La_7Au_3 compound (*hP*20-Th_7Fe_3) was recently reported by Ovchinnikov et al.[8]

The only Mg-Au binary compound involved in this study is $AuMg_3$, congruently melting at 818°C. The crystal structure of this compound was revised several times after its first investigation from XRD powder diffraction[9]; a hexagonal acentric structural model (*hP*24-Cu_3P) was finally established for it from single crystal studies[10], being a superstructure of that proposed in the pioneering work.

Only the stoichiometric equiatomic phase LaAuMg (*hP*9-ZrNiAl) is reported in the literature[11] in the compositional range of interest.

Table S1. SEM/EDXS (at.%) and XRD data on the investigated La-Au-Mg samples (if not specified, samples were annealed at 400 °C).

Nr.	Nominal comp. EDXS comp.	Phases	EDXS comp. La; Au; Mg	Crystal structure	Lattice parameters *(nm)*		
					a	***b***	***c***
1	$La_3Au_7Mg_{90}$ $La_{3.9}Au_{7.7}Mg_{88.4}$	$LaMg_{12-x}$ $AuMg_3$ (Mg)	8.5; 1.1; 90.4 0.6; 25.3; 74.1 1.5; 1.8; 96.7	*oI*346-10.32-$LaMg_{\sim 11}$ *hP*24-Cu_3P *hP*2-Mg	1.0329(8) 0.8059(3) 0.3206(1)		0.772(1) 0.8472(6) 0.5201(2)
2	$La_8Au_7Mg_{85}$ $La_{9.2}Au_{7.0}Mg_{83.8}$	$La_2(Mg,Au)_{17}$ τ_1–$La_{1.82}Au_{3+x}Mg_{14.36-x}$ $AuMg_3$	10.0; 2.9; 87.1 9.6; 16.4; 74.0 0.4; 26.9; 72.7	*hP*42-x-$CeMg_{10.3}$ *hP*42-x-$CeMg_{10.3}$ *hP*24-Cu_3P	1.0263(6) 0.9944(4) 0.8064(3)		1.0229(5) 0.9947(6) 0.8472(5)
3	$La_{16}Au_4Mg_{80}$ $La_{16.8}Au_{3.7}Mg_{79.5}$	$LaMg_3$ $La_2(Mg,Au)_{17}$ τ_1–$La_{1.82}Au_{3+x}Mg_{14.36-x}$	24.4; 0.5; 75.1 11.2; 1.8; 87.0 11.4; 14.6; 74.0	*cF*16-BiF_3 *hP*42-x-$CeMg_{10.3}$ *hP*42-x-$CeMg_{10.3}$	0.74930(3) 1.0329(1) 0.9986(2)		 1.0174(3) 0.9907(3)
4	$La_{17}Au_{10}Mg_{73}$ $La_{18.6}Au_{10.4}Mg_{71.0}$	$LaMg_3$ τ_1–$La_{1.82}Au_{3+x}Mg_{14.36-x}$ τ_2-$La_3Au_{4-x}Mg_{12+x}$	26.0; 0.2; 73.8 11.7; 16.9; 71.4 17.9; 15.5; 66.5	*cF*16-BiF_3 *hP*42-x-$CeMg_{10.3}$ *hP*38-$Gd_3Ru_4Al_{12}$	0.7495(2) 0.9958(6) *not measurable*		 0.9871(7)
5	$La_7Au_{18}Mg_{75}$ $La_{8.4}Au_{19.2}Mg_{72.4}$	$AuMg_3$ τ_1–$La_{1.82}Au_{3+x}Mg_{14.36-x}$ $La_2(Mg,Au)_{17}$*	0.2; 31.9; 67.9 10.4; 16.4; 73.2 9.8; 4.0; 86.2	*hP*24-Cu_3P *hP*42-x-$CeMg_{10.3}$ *hP*42-x-$CeMg_{10.3}$	0.8076(2) 0.9930(4) *not measurable*		0.8489(4) 0.9957(2)
6	$La_{11.5}Au_{16}Mg_{72.5}$ $La_{12.4}Au_{17.9}Mg_{69.8}$	τ_1–$La_{1.82}Au_{3+x}Mg_{14.36-x}$ τ_2-$La_3Au_{4-x}Mg_{12+x}$ $LaMg_3$*	11.2; 17.6; 71.2 17.1; 19.6; 63.3 26.3; 0.0; 73.7	*hP*42-3.66-$CeMg_{10.3}$ *hP*38-$Gd_3Ru_4Al_{12}$ *cF*16-BiF_3	0.9961(6) 0.9765(3) *not measurable*		0.989(1)
7	$La_{24}Au_{18}Mg_{58}$ $La_{24.2}Au_{16.5}Mg_{59.3}$	τ_3-$LaAuMg_2$ τ_2-$La_3Au_{4-x}Mg_{12+x}$ $LaMg_3$ τ_4-$LaAu_{1+x}Mg_{1-x}$*	26.4; 26.6; 47.0 17.3; 17.7; 65.0 26.3; 0.5; 73.2 34.2; 34.4; 31.4	*oS*16-$MgCuAl_2$ *hP*38-$Gd_3Ru_4Al_{12}$ *cF*16-BiF_3 *hP*9-ZrNiAl	0.4524(2) 0.9782(9) 0.74816(8) 0.7792(6)	1.0614(4)	0.8097(2) 1.039(3) 0.4253(3)
8#	$La_{17}Au_{18}Mg_{65}$ $La_{20.0}Au_{21.2}Mg_{58.8}$	τ_3-$LaAuMg_2$ τ_2-$La_3Au_{4-x}Mg_{12+x}$ τ_1–$La_{1.82}Au_{3+x}Mg_{14.36-x}$ τ_4-$LaAu_{1+x}Mg_{1-x}$	26.2; 27.1; 46.7 17.1; 19.5; 63.4 11.5; 17.3; 71.2 33.8; 35.2; 30.9	*oS*16-$MgCuAl_2$ *hP*38-$Gd_3Ru_4Al_{12}$ *hP*42-3.66-$CeMg_{10.3}$ *hP*9-ZrNiAl	0.4518(3) 0.9787(5) 0.9953(9) *not measurable*	1.0614(4)	0.8094(2) 1.0415(9) 0.9867(7)
9#	$La_{25}Au_{25}Mg_{50}$ $La_{23.0}Au_{22.9}Mg_{54.1}$	τ_3-$LaAuMg_2$ τ_4-$LaAu_{1+x}Mg_{1-x}$ τ_2-$La_3Au_{4-x}Mg_{12+x}$ τ_1–$La_{1.82}Au_{3+x}Mg_{14.36-x}$	25.8; 26.8; 47.5 33.5; 35.1; 31.4 16.8; 22.1; 61.2 11.4; 17.4; 71.2	*oS*16-$MgCuAl_2$ *hP*9-ZrNiAl *hP*38-$Gd_3Ru_4Al_{12}$ *hP*42-3.66-$CeMg_{10.3}$	0.45228(7) 0.78002(8) 0.9718(2) *not measurable*	1.0631(1)	0.8105(1) 0.42554(7) 1.0372(3)
10	$La_{30}Au_{10}Mg_{60}$ $La_{31.6}Au_{11.5}Mg_{56.8}$	$LaMg_3$ τ_4-$LaAu_{1+x}Mg_{1-x}$ $LaMg_2$	71.8; 0.4; 27.8 34.5; 32.7; 31.8 *not measurable*	*cF*16-BiF_3 *hP*9-ZrNiAl *cF*24-$MgCu_2$	0.7514(1) 0.7816(1) 0.88078(8)		 0.4259(1)
11	$La_{37}Au_{10}Mg_{53}$ $La_{37.8}Au_{8.9}Mg_{53.3}$	$LaMg_2$ $LaMg$ τ_4-$LaAu_{1+x}Mg_{1-x}$	35.0; 0.0; 65.0 47.8; 0.0; 52.2 34.6; 32.7; 32.7	*cF*24-$MgCu_2$ *cP*2-CsCl *hP*9-ZrNiAl	0.8800(1) 0.3961(2) 0.7810(3)		 0.4259(3)
12	$La_{60}Au_3Mg_{37}$ $La_{61.0}Au_{2.5}Mg_{36.5}$	$LaMg$ (La) τ_4-$LaAu_{1+x}Mg_{1-x}$	54.9; 0.2; 44.9 96.3; 0.3; 3.4 *not measurable*	*cP*2-CsCl *hP*4-Nd *hP*9-ZrNiAl	*scarce quality of XRD pattern, sufficient only for phase identification*		
13	$La_{73}Au_{10}Mg_{17}$ $La_{72.6}Au_{9.6}Mg_{17.8}$	(La) τ_4-$LaAu_{1+x}Mg_{1-x}$ $LaMg$	96.3; 0.4; 3.3 36.2; 34.1; 29.7 53.6; 0.2; 46.2	*hP*4-Nd *hP*9-ZrNiAl *cP*2-CsCl	*scarce quality of XRD pattern, sufficient only for phase identification*		
14	$La_{56}Au_{27}Mg_{17}$ $La_{57.3}Au_{26.5}Mg_{16.2}$	(La) τ_4-$LaAu_{1+x}Mg_{1-x}$ La_2Au	98.9; 0.6; 0.5 35.2; 34.8; 30.0 65.4; 33.5; 1.1	*hP*4-Nd *hP*9-ZrNiAl *oP*12-Co_2Si-b	0.3770(2) 0.7818(2) 0.742(2)	 0.5117(6)	1.2158(8) 0.4262(2) 0.940(1)
15	$La_{71}Au_{25}Mg_4$ $La_{66.5}Au_{27.9}Mg_{5.6}$	La_2Au (La) τ_4-$LaAu_{1+x}Mg_{1-x}$ τ_5~$La_{55}Au_{40}Mg_5$*	63.9; 35.1; 1.0 97.5; 0.3; 2.3 *not measurable* 54.9; 41.7; 3.4	*oP*12-Co_2Si-b *hP*4-Nd *hP*9-ZrNiAl *tP*10-U_3Si_2	0.743(4) 0.376(1) *not measurable* *not measurable*	0.512(5)	0.940(1) 1.216(4)
16	$La_{50}Au_{40}Mg_{10}$ $La_{49.0}Au_{40.0}Mg_{11.0}$	LaAu τ_5~$La_{55}Au_{40}Mg_5$ τ_4-$LaAu_{1+x}Mg_{1-x}$	49.4; 49.7; 0.9 53.6; 40.9; 5.5 35.4; 35.0; 29.6	*oP*8-FeB-b *tP*10-U_3Si_2 *hP*9-ZrNiAl	*scarce quality of XRD pattern, sufficient only for phase identification*		
17	$La_{50}Au_{40}Mg_{10}$ $La_{48.9}Au_{41.1}Mg_{10.0}$	LaAu τ_5~$La_{55}Au_{40}Mg_5$ τ_4-$LaAu_{1+x}Mg_{1-x}$ La_2Au*	47.5; 50.7; 1.8 52.8; 40.9; 6.3 37.0; 34.9; 28.1 66.1; 33.6; 0.3	*oP*8-FeB-b *tP*10-U_3Si_2 *hP*9-ZrNiAl *oP*12-Co_2Si-b	 ~0.830 0.780(1) *not measurable*		 ~0.404 0.427(5)

18	$La_{55}Au_{42}Mg_3$ $La_{51.3}Au_{44.2}Mg_{4.5}$	La_2Au LaAu τ_5~$La_{55}Au_{40}Mg_5$ α-(La)*	64.7; 34.5; 0.8 48.5; 50.2; 1.3 53.7; 41.7; 4.6 96.8; 3.2; 0.0	*oP*12-Co_2Si-b *oP*8-FeB-b *tP*10-U_3Si_2 *hP*4-Nd	*scarce quality of XRD pattern, sufficient only for phase identification*

* – out of equilibrium phase, small amount # – samples obtained by controlled thermal treatment

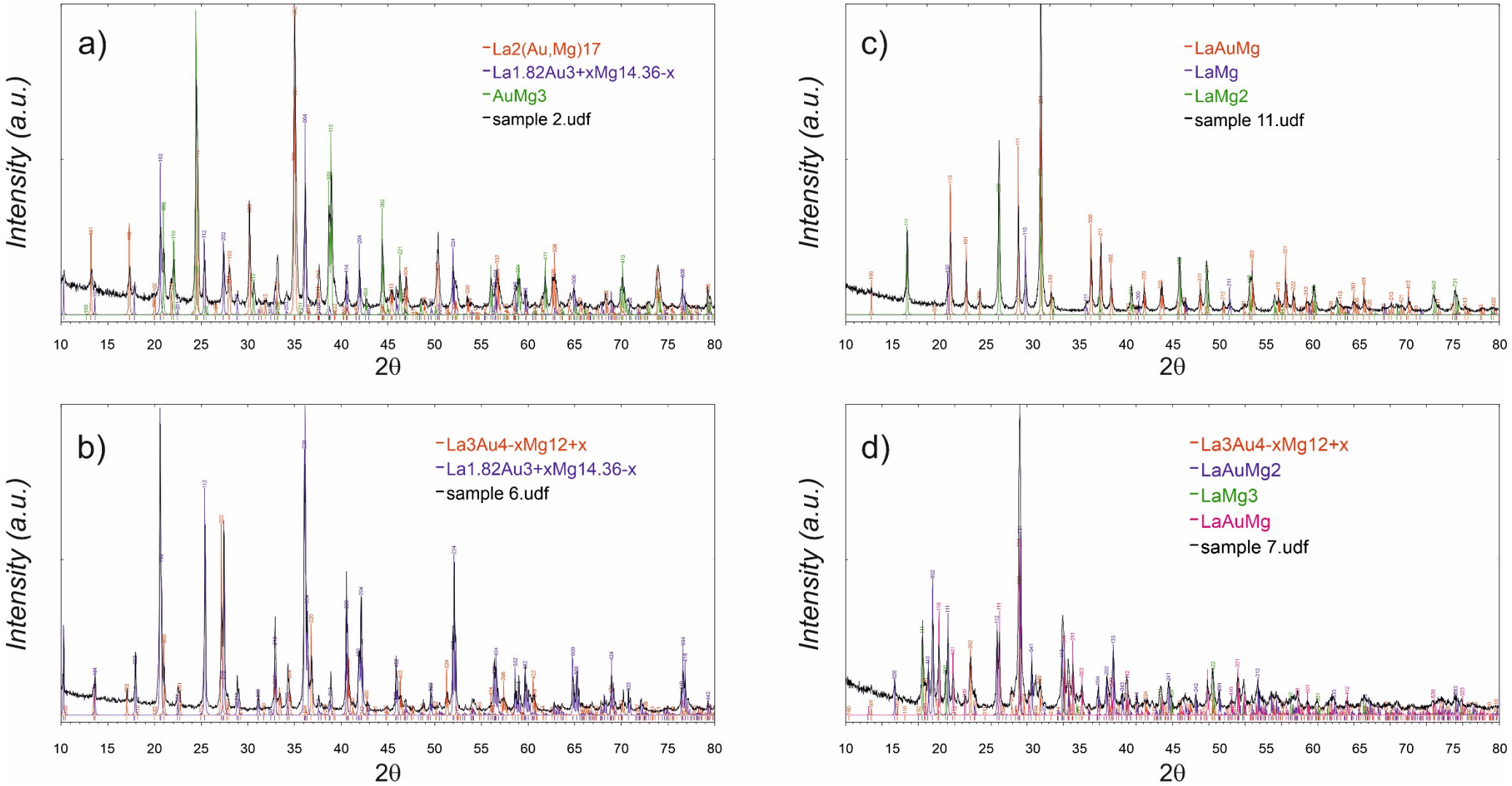

Figure S1. Calculated (colored lines) and experimental (black line) powder diffraction pattern profiles for selected La-Au-Mg samples.

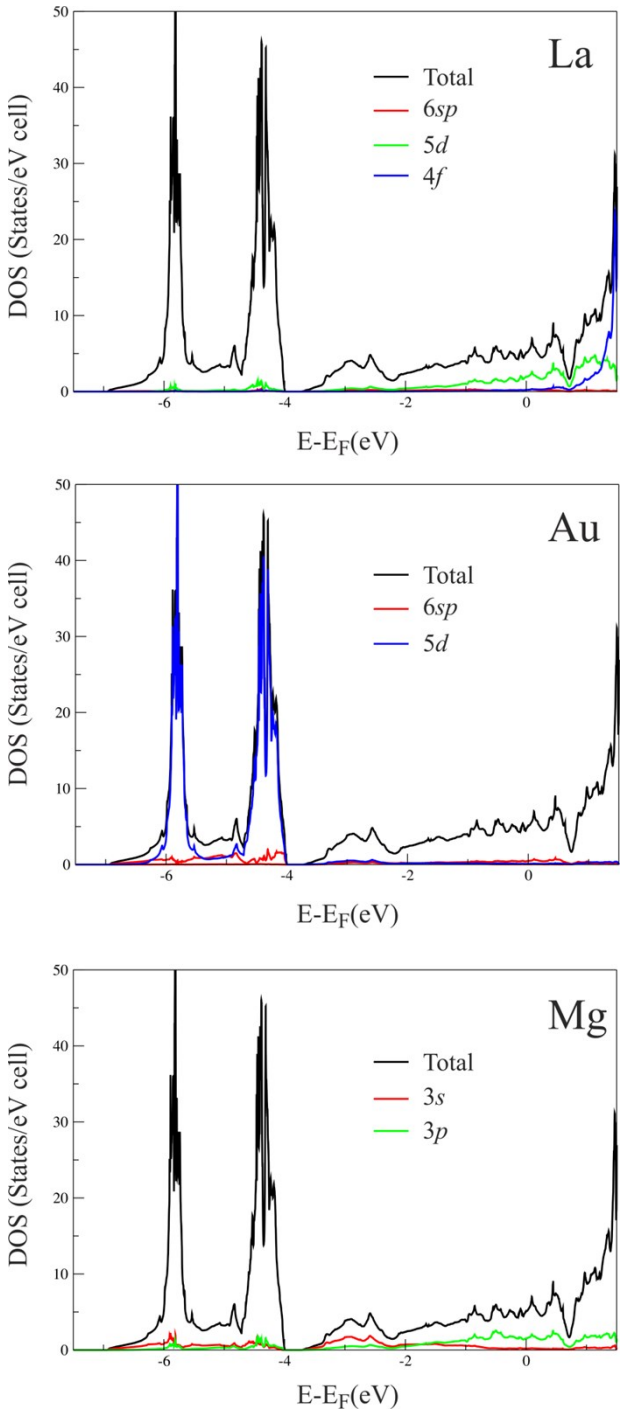

Figure S2. Calculated orbital-projected DOS for La, Au and Mg in fully relativistic approximation for $LaAuMg_2$.

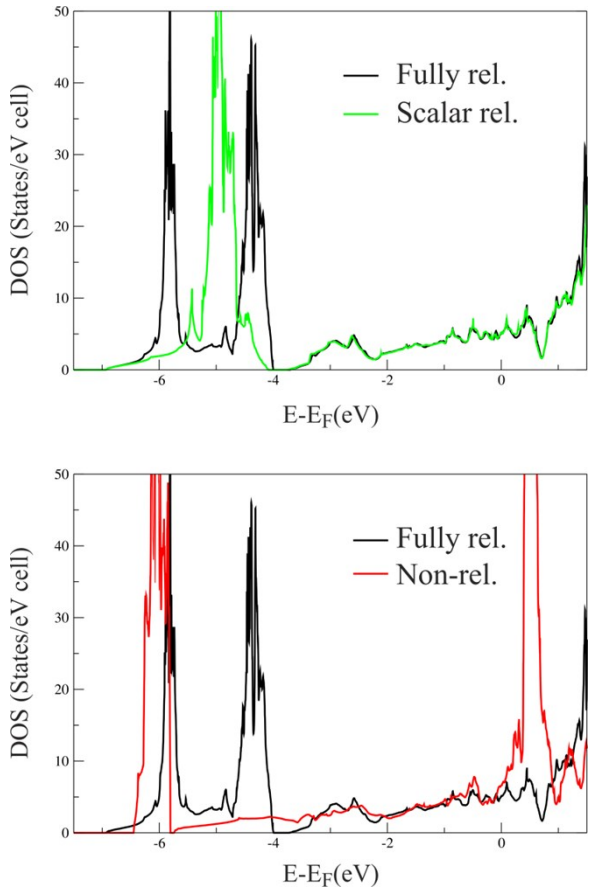

Figure S3. Comparison between the total DOS calculated in fully relativistic (black curve), scalar relativistic (green) and non-relativistic (red) approximation.

In the scalar relativistic calculation, where the spin-orbit interactions are not included, the two peaks at about -6 and -4 eV merge into one around -5 eV.

A quite different trend is observed for the non-relativistic curve; in particular, the 5*d* states are shifted towards lower energy due to the missing relativistic inner shells contraction which results in a reduced effective nuclear charge (Z_{eff}). This effect, also known as *indirect relativist effect*, leads to a relevant destabilization (shift at higher energy) and expansion for the outer and more diffuse *f*- and *d*-orbitals [12].

Table S2. QTAIM effective charges and atomic basins volume obtained on the basis of electron densities resulting from non-relativistic and scalar-relativistic calculations.

Species X	Non-relativistic		Scalar-relativistic	
	$Q^{eff}(X)$	$V(X)$	$Q^{eff}(X)$	$V(X)$
La	+0.90	198.6	+1.06	194.0
Au	–2.48	272.4	–2.72	282.1
Mg	+0.79	99.8	+0.83	97.3

Table S3. ELI-D valence basin population $\bar{N}(B_i)$, bond fractions and effective atomicity for A, B and C basins (see figure 5 in the main text) obtained from the non-relativistic calculation. To make the comparison easier Table 3 from the main text is also reported.

Non-relativistic					
ELI-D basin (B_i)	*Effective atomicity* $Mg_2Au_2La_x$	$\bar{N}(B_i)$	$\sum_j^2 p(B_i^{Mg_j})$	$\sum_j^2 p(B_i^{Au_j})$	$\sum_j^x p(B_i^{La_j})$
A	$Au_2Mg_2La_2$ (6*a*)	1.680	0.197	0.723	0.060
B	$Mg_2La_4Au_2$ (8*a*)	2.215	0.585	0.203	0.210
C	$Au_2Mg_2La_3$ (7*a*)	1.658	0.239	0.670	0.091

Scalar-relativistic					
ELI-D basin (B_i)	*Effective atomicity* $Mg_2Au_2La_x$	$\bar{N}(B_i)$	$\sum_j^2 p(B_i^{Mg_j})$	$\sum_j^2 p(B_i^{Au_j})$	$\sum_j^x p(B_i^{La_j})$
A	$Au_2Mg_2La_2$ (6*a*)	2.193	0.134	0.800	0.057
B	$Mg_2La_4Au_2$ (8*a*)	2.147	0.620	0.109	0.249
C	$Au_2Mg_2La_3$ (7*a*)	1.328	0.230	0.687	0.083

Table S4. Population of ELI-D core basins. *n* denotes the main quantum number.

	Species X	$\sum_{i=1}^{n-1} \bar{N}_i^{ELI}(X)$	N_{core}
Non-rel.	Mg	10.065	10
	La	55.236	54
	Au	77.549	77*
Scalar-rel.	Mg	10.063	10
	La	54.957	54
	Au	77.072	77*

*Assuming a [Xe] $4f^{14}$ $5d^9$ $6s^2$ electronic configuration for Au.

Table S5. Average population of gold penultimate shell ELI-D basins together with the population of their portions intersected by La atoms. *n* denotes the main quantum number.

	$\bar{N}_{n-1}^{ELI}(Au)$	$\bar{N}(Au^{Au})$	$\bar{N}(Au^{La})$ 0.307 nm	$\bar{N}(Au^{La})$ 0.320 nm
Non-rel.	18.580	18.555	0.008	0.008
Scalar-rel.	18.697	18.649	0.028	0.010

Summarizing, relativistic effects leads to:

1) increasing charge transfer between La and Au; that of Mg is practically unaffected (Table S2);
2) increasing of A-basins population and decreasing of the C basins population of about 0.5 and 0.3 e, respectively. The B population is practically the same. The number and location of ELI-D attractors (and related basins) is the same (Table S3);
3) the same effective atomicities. In all cases, La contributions doesn't change noticeably. The Mg contribution to B-basins increases and decreases in the A-one; the Au behavior is opposite. The contribution to the C-basins doesn't change noticeably (Table S3);
4) increasing of the number of the electrons in the valence region from 7.23 to 7.86 e/f.u.. This effect is caused by a reduced storage (in the scalar relativistic treatment) of electrons in La and Au core region. Population of Mg core is the same (Table S4);
5) more covalent Au–La bonding. In fact, gold bulges are bigger and more intersected by La QTAIM atoms (Table S).

References

1 A. Berche, P. Benigni, J. Rogez and M. C. Record, *J. Therm. Anal. Calorim.*, 2012, 107, 797–807.

2 P. Manfrinetti and K. A. Gschneidner, *J. Less-Common Met.*, 1986, **123**, 267–275.

3 M. Giovannini, A. Saccone, R. Marazza and R. Ferro, *Metall. Mater. Trans. A*, 1995, **26**, 5–10.

4 S. De Negri, P. Solokha, V. Pavlyuk and A. Saccone, *Intermetallics*, 2011, **19**, 671–681.

5 R. V. Denys, A. A. Poletaev, J. K. Solberg, B. P. Tarasov and V. A. Yartys, *Acta Mater.*, 2010, **58**, 2510–2519.

6 T. B. Massalski, H. (Hiroaki) Okamoto and ASM International., *Binary alloy phase diagrams*, ASM International, 1990.

7 H. Q. Dong, X. M. Tao, H. S. Liu, T. Laurila and M. Paulastro-Kröckel, *J. Alloys Compd.*, 2011, **509**, 4439–4444.

8 A. Ovchinnikov and A.-V. Mudring, in *Exploratory studies in the intermetallic RE–Mn–Au systems (RE = rare-earth metal), 17th European Conference on Solid state Chemistry*, Lille, France, 2019, p. P85.

9 K. Schubert and K. Anderko, *Z. Met.*, 1951, **42**, 321–325.

10 K. J. Range and P. Hafner, *J. Alloys Compd.*, 1993, 191, L5–L7.

11 R. Pöttgen, R.-D. Hoffmann, J. Renger, U. C. Rodewald and M. H. Möller, *Zeitschrift fur Anorg. und Allg. Chemie*, 2000, **626**, 2257–2263.

12 P. Schwerdtfeger and M. Lein, in *Gold Chemistry*, Wiley-VCH Verlag GmbH & Co. KGaA, Weinheim, Germany, 2009, pp. 183–247.